Phonon Bottleneck Identification in Disordered Nanoporous Materials

Giuseppe Romano[*] and Jeffrey C. Grossman[†]
Department of Materials Science and Engineering,
Massachusetts Institute of Technology, 77 Massachusetts Avenue, Cambridge, MA 02139

Nanostructured materials are promising as thermoelectrics since thermal transport can be suppressed with little degradation in electrical properties, a crucial requirement for high-efficiency thermal energy conversion. Porous materials offer a flexible platform thanks to their extensive range of possible configurations and robust nature compared to other nanostructures. Although there has been great progress in modeling the thermal properties of nanoporous materials, it has remained a challenge to screen such materials over a large phase space due to the slow simulation time required for accurate results. This has left a gap in our ability to optimize nanoporous thermoelectrics both in designing ordered, ideal porous structures as well as in understanding the role of pore disorder. In this work, we use density functional theory in connection with the Boltzmann transport equation, to perform high-throughput calculations of heat transport in disordered porous materials. By leveraging graph theory and regressive analysis, we identify the set of pores representing the most effective phonon bottleneck. The strength of such bottlenecks is assessed by the "repeated bottleneck" algorithm, which ultimately provides a measure of the effect of disorder on thermal transport. These results shed light on thermal conductivity reduction in disordered porous materials and provide a simple tool to estimate phonon suppression in realistic porous materials.

INTRODUCTION

The efficient and inexpensive conversion of heat directly into electricity is a long-sought goal with enormous potential in the clean-energy technology landscape [1]. The engineering of thermoelectric materials, however, is particularly challenging because of the interrelation of key physical properties constituting the thermoelectric figure of merit ZT, defined as $ZT = \frac{T\sigma S^2}{\kappa}$ where σ is the electrical conductivity, κ is the lattice thermal conductivity, S is the Seebeck coefficient, and T the temperature. A powerful way to decouple the electrical and thermal transport is given by nanostructuring. In most semiconductors, the numerator of ZT, also referred to as "power factor", is maximized at relatively high carrier concentrations so the dominant electron mean free path (MFP) can be as small as few nanometers [2]. Conversely, phonons may have much larger MFPs, even on the order of microns [3]. Properly engineered nanostructures are therefore able to scatter phonons more effectively than electrons. Porous materials offer a highly tunable platform thanks to great degree of structural tunability including pore size, shape and arrangement, as well as the potential for controllable uniform thin films, high temperature resilience and and robust contacts. As an example, the thermal conductivities of nanoporous Si have been measured in many studies with the common finding of a strong suppression of thermal transport, leading to a significant improvement in experimentally measured ZT [4–8]. On the computational level, several models based on the Boltzmann Transport Equation (BTE) have also shown low thermal conductivities and revealed important features of phonon-boundary scattering and fundamental thermal transport in nanoporous materials [9–11]. Preliminary attempts aiming at tuning thermal conductivity in nanoporous Si have shown that, even within ordered configurations and with pores of the same size, the pattern in the pores can have a large influence on the resulting thermal transport [12]. Although aligned configurations offer a robust platform for controllable experiments, pore disorder is unavoidable, especially at smaller length scales [13]. Recent Monte Carlo calculations [14, 15] investigated thermal transport in disordered porous materials with circular pores and concluded that the density of porous along the heat flux direction has a significant influence on thermal conductivity. In this work, we expand on this concept by developing a method that identifies the actual set of pores representing the highest local resistance to phonon transport. To this end, we use the recently developed first-principles BTE solver [16] to perform high-throughput calculations of thermal transport in random-pore configurations with pores of circular and square shapes. Then, we establish a correlation between the phonon suppression and the pore arrangement within given configuration, leading to the identification of the pores constituting the phonon bottleneck. Upon introducing a simple descriptor representing the strength of this collection of pores, we find a correlation between such a parameter and the effective thermal conductivity κ_{eff}. Last, we estimate the effect of pore disorder on thermal transport by means of the "repeated-bottleneck" algorithm, a method that classifies strong and weak phonon bottlenecks. This work can be potentially used to estimate the degree of phonon suppression in realistic nanoporous samples while avoiding the computational burden of solving the BTE.

PHONON BOLTZMANN TRANSPORT EQUATION

Our computational approach is based on recent implementation of the BTE for phonons, which under the relaxation time approximations, reads as [11]

$$\Lambda \hat{\mathbf{s}}(\Omega) \cdot \nabla T(\mathbf{r}, \Omega, \Lambda) + T(\mathbf{r}, \Omega, \Lambda) = \gamma \int \frac{K(\Lambda)}{\Lambda'^2} < T(\mathbf{r}, \Omega, \Lambda') > d\Lambda', \quad (1)$$

where $K(\Lambda)$ is the bulk MFP distribution, $T(\mathbf{r}, \hat{\mathbf{s}}, \Lambda)$ is the temperature associated to phonons with MFP Λ, $\hat{\mathbf{s}}$ is the phonon direction, $\gamma = \left[\int K(\Lambda)/\Lambda^2 d\Lambda \right]^{-1}$ and $< . >$ is an angular average. The RHS of Eq. 1 is the effective lattice temperature, a quantity describing the average phonon energy. The term $K(\Lambda)$ is obtained by using harmonic and anharmonic forces in connection with density functional theory [3, 17]. The spatial discretization of Eq. 1 is achieved by the Finite-Volume (FV) method. The simulation domain is discretized by means of an unstructured mesh, computed by GMSH [18]. The phonon BTE requires the solid angle discretization, as well, in order to account for different phonon directions. We use the Discrete Ordinate Method (DOM), a technique that essentially solves the BTE for each phonon direction independently and then combines the solutions by an angular integration [19]. As Si is a non-gray material, we need to include the whole MFP distribution, which leads to a discretization in the MFP space. In this study we solve the BTE for 30 MFPs and 576 phonon directions over a mesh with about 6500 elements. The actual algorithm is detailed in [20]. The overall solution of Eq. 1 requires solving the BTE thousands of times, leading to an increase in the computational time. However, our solver has been conveniently parallelized and each configuration takes only few minutes with a cluster of 32 nodes.

The walls of the pores are assumed diffusive, a condition that translates into

$$T_b = -\frac{\int_{\Omega^+} \int (K(\Lambda)/\Lambda) \, T(\mathbf{r}, \Omega, \Lambda) \hat{\mathbf{s}}(d\Omega) \cdot \hat{\mathbf{n}} \, d\Omega d\Lambda}{\int_{\Omega^-} \int (K(\Lambda)/\Lambda) \, \hat{\mathbf{s}}(d\Omega) \cdot \hat{\mathbf{n}} \, d\Omega d\Lambda}, \quad (2)$$

where Ω^- and Ω^+ are the solid angle for incoming and outgoing phonons with respect to the contact with normal $\hat{\mathbf{n}}$. Once Eq. 1 is solved, thermal flux is computed via $\mathbf{J}(\mathbf{r}) = 3 \int K(\Lambda)/\Lambda < T(\mathbf{r}, \Omega, \Lambda) \hat{\mathbf{s}} > d\Lambda$. The effective thermal conductivity is obtained by using Fourier's law, i. e. $\kappa_{eff} = (L/\Delta T) \int_{hot} < \mathbf{j}(\mathbf{r}, \Omega, \Lambda) \hat{\mathbf{n}} > dS$, where $\Delta T = 1$ K is the applied temperature and K is the distance between the hot and cold contacts (or the size of the unit-cell).

ALIGNED PORES

We first compute thermal transport in aligned configurations, which we will refer to as AC and AS, depending on whether the pores are square or circular, respectively. The unit-cell comprises a single pore and is a square with size L = 10 nm. Heat flux is enforced by applying a difference of temperature $\Delta T = 1$ K along the x direction. The porosity is fixed at $\phi = 0.25$, and periodic boundary conditions are applied throughout. The computed values for κ_{eff} are 6.37 and 6.67 W m^{-1} K $^{-1}$ for AC and AS, respectively. These values, which are considerably lower than the bulk value 156 Wm^{-1}K^{-1}, are consistent with those computed in our previous studies [21]. Using a Finite-Volume diffusive heat conduction solver, we also compute thermal transport in absence of phonon-boundary scattering, obtaining significantly higher values (93.05 and 88.26 W m^{-1} K $^{-1}$ for AC and AS, respectively). Such results, as expected, reveal strong phonon suppression due to phonon size effects. From the magnitude of the thermal flux, which is shown in the upper half of Fig. 1, we note that the areas with higher thermal flux are near the spaces between pores perpendicular to the applied temperature gradient.
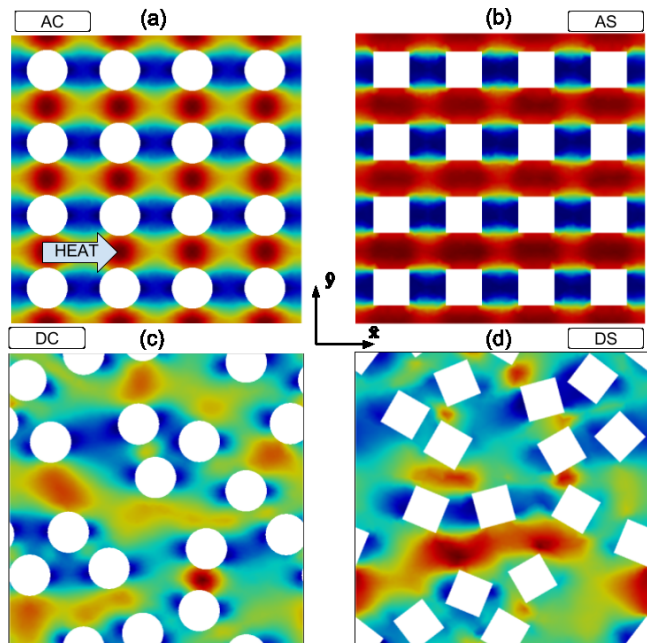

FIG. 1. Magnitude of thermal flux. Red and blue areas refer to high-flux and low-flux regions, respectively. The temperature gradient is imposed along the x-direction. In (a) and (b), we show AC and AS, respectively. Phonons prefer to travel in the spaces between the pores, as highlighted by the red areas. In (c) and (d), we show DC and DS, respectively. In all the configurations the pores arrangement is periodic in both x and y direction.

RANDOM PORES

For random-pore (or disordered) configurations, the size of the unit-cell is chosen to be L = 40 nm, four times as large as that for the aligned cases. Non-overlapping pores are randomly generated while keeping the porosity fixed. As the area of the pores is the same as that of the aligned arrangement, we have 16 pores within each configuration. We compute κ_{eff} for three hundreds arrangements, one hundred for each shape, which we refer to as DC and DS. The magnitude of thermal flux for three configurations, one for each shape, is shown in the lower part of Fig. 1. We note that the formation of high-flux regions is irregular as it depends on the randomly chosen pore configuration. In the upper part of Fig. 2 we show the κ_{eff} distributions obtained by Fourier's law. We can observe variations within 5% from the average value, due exclusively to geometric effects arising from material removal. The average values of κ_{eff} for DC and DS are near that of their aligned counterparts. We pointed out that this small variation in κ_{eff} motivates us to keep the porosity fixed. If we assume that electrons travel diffusively, the electrical conductivity will have a similar variation because of the same diffusive-like physics underlying macroscopic transport of electrons and phonons [22]. Consequently, a decrease in κ_{eff} due to size effects with no change in porosity will most likely translate into an increase in ZT. When size effects are switched on in the simulation, we see that pore disorder plays an important role. Specifically, the DC and DS cases are found to have average κ_{eff} values 15 % and 30 % lower, respectively, than that of their aligned counterparts. These trends can be understood by analyzing the geometries of the random structures, as explained in the next section.

IDENTIFICATION OF A DESCRIPTOR

Here we attempt to correlate geometrical features to κ_{eff}. In previous work [12], we reported that κ_{eff} in nanoporous materials is dictated by the *view factor* and the pore-pore distances. We note that the *view factor* is a geometrical feature that describes the ability of a ray to travel across the simulation domain without intercepting the pores [23]. In random-pore configurations, the view factor generally vanishes because of the disordered pores blocking all the direct path across the unit-cell. It is natural, therefore, to speculate whether the average pore-pore distance in the disordered configurations is correlated with κ_{eff}. However, after a regression analysis, we conclude that unlike for the ordered case, such a parameter has only a marginal role for the disordered systems. In fact, rigorously speaking, only the inter-pore spaces perpendicular to heat flux matter. In search of a more meaningful parameter, we hypothesize that for a generic arrangement we can model heat transport as a
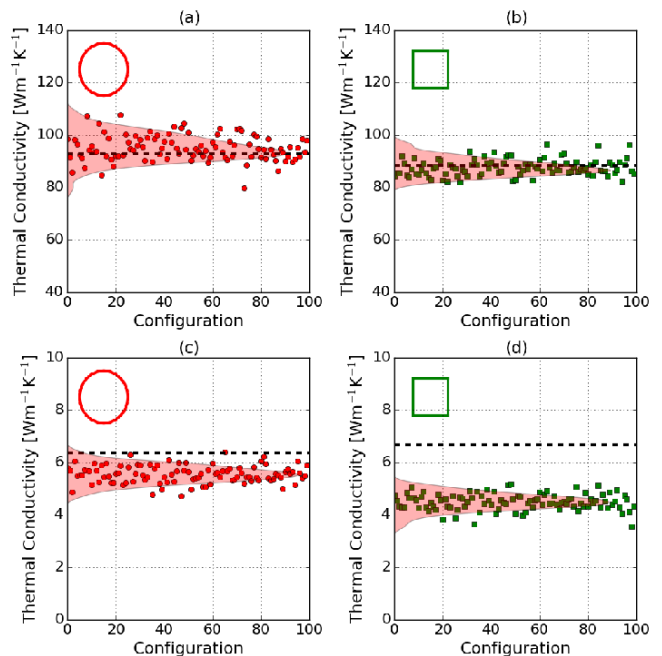

FIG. 2. The diffusive κ_{eff} distributions for DC (a) and DS (b) have mean values that are close to κ_{eff} of their aligned counterparts, depicted by dotted lines. The values for κ_{eff} computed by the BTE for DC (c) are slightly smaller than of AC, while disorder significantly degrades thermal transport in DS (d).

network of resistances. Within this assumption, we aim to identify the set of pores that forms the highest resistance perpendicular to the heat flux. To this end, we first calculate all the possible "pore-paths" perpendicular to the applied temperature gradient, and then we compute the sum of the pore-pore distances within each set of pores. The distances between adjacent pores is conveniently described by the *first-neighbor* map, which is computed as follows. Say the two pores are P1 and P2, we compute their distance by following three simple steps:

1. We compute the circumcenter of the two points, C_1 and C_2.

2. We discretized the distance between the two circumcenters, i.e $\overline{C_1 - C_2} = 100\Delta d$.

3. If the two pores intersect, then the distance d_{12} is the total distance traveled by P_1 until the intersection. If the two pores do not intersect, we go back to point 2. If P_1 intersects a pore other than P_2 then P_1 and P_2 are not neighbors and another pores pair will be chosen.

The intersection among polygons is computed by the package PyClipper [24].
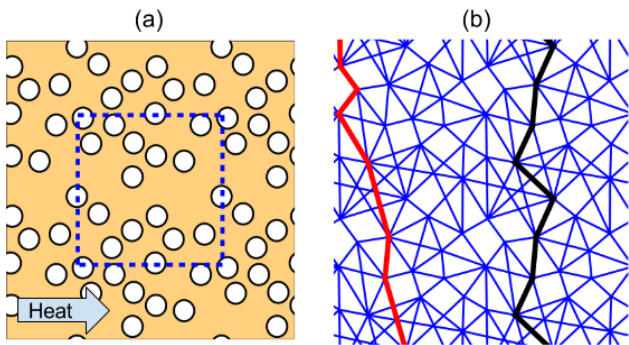
FIG. 3. (a) A random pores configuration is shown in a alongside the unit-cell, depicted by the dotted line. The first-neighbor map (b) highlights connection between pores that can reach each other with no interference from other pores. The red path is skew with respect to heat transport so it is discarded. Conversely, the black path is perpendicular to heat flux and, as such, is a potential bottleneck.

An example of first-neighbor map is shown in Fig. 3. A potential phonon bottleneck is a collection of pores forming a path that is perpendicular to the applied temperature gradient. In order to identify such pores, we build a directed graph G describing the connections of a pore with the set of neighbors located at higher y-coordinate. As the pores arrangement is periodic in both x and y-axis, there exist paths on G that are periodic, as well. All the periodic routes, called "cycles", are calculated using Johnson's algorithm [25] implemented in NetworkX [26]. Although the number of cycles in each configuration can easily reach few thousands, not all of them are practical for our purposes. We rule out the cycles that are skewed with respect to the applied temperature gradient, as shown in Fig. 5-b. After this screening, the average number of cycles becomes few hundreds, an amenable number for the subsequent analysis. In order to identify the bottleneck for each configuration we develop the following algorithm:

1. For each cycle, $C = C_1, C_2...C_n$, we compute the inter-pore distance of its constituting pores, $R_n = R_1, R_2...R_p$, where p is the number of each cycle. Then, we compute the sum of such distances, i.e. $D_n = \sum_n R_n$.

2. From the previous point, we have the set $D = D_1, D_2...D_n$. The bottleneck is then $d = \min\{D\}$.

As shown from the upper half of Fig. 4, κ_{eff} has a good correlation with d. The effectiveness of d in describing nanoscale thermal transport in such structures can be estimated by the Spearman correlation rank, a quantity that describes how two variables are monotonically correlated to each other [27]. For DC and DS, we obtain a significant Spearman correlation (higher than 0.6), sug-

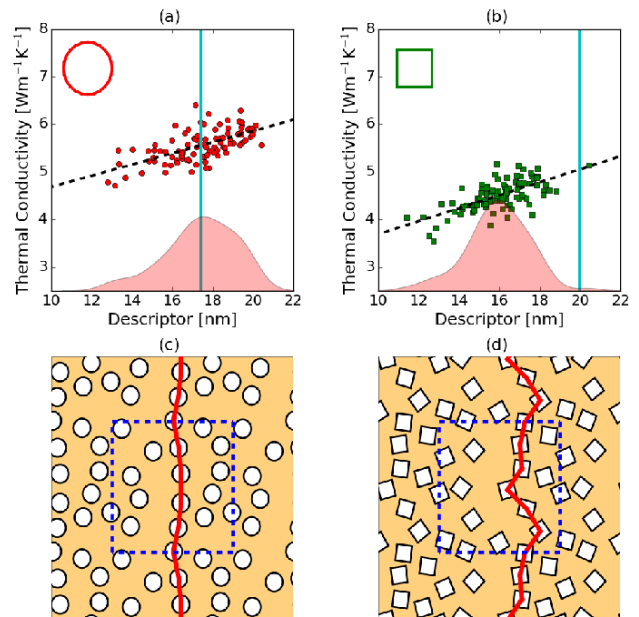gesting that d can be used as a good *descriptor*. We

FIG. 4. Thermal conductivity distributions versus the size of the phonon bottleneck for DC (a) and DS (b). A linear fitting and the bottleneck distributions are also shown. The cyan line is the pore-pore distance for the correspondent aligned configurations. The set of pores associated to the most effective bottleneck for DC and DS are shown in (c) and (d), respectively.

recall that a descriptor is a simple quantity that can be used to estimate another quantity, which is challenging to compute. Therefore, descriptors are powerful tools for high-throughput, computationally-intensive calculations. These results explain the trends in the κ_{eff} if we compare the distribution of d with respect to the sum of the pore-pore distances in the aligned configurations, both shown in the upper part of Fig. 4. According to simple geometric considerations, we have $d_{AC} = 4L(1 - 2\sqrt{\phi/\pi}) = 17.44$ nm and $d_{AS} = 4L(1 - \sqrt{\phi}) = 20$ nm. For DC, roughly half of the configurations have d lower than d_{AC} while for DS, almost all the configurations have d smaller than that of AS. For these two cases, the combined effect of small bottleneck and vanishing view factor significantly lowers κ_{eff}. This predominance of the pore-pore distance over the view factor is consistent with previous work [12]. We note that most of the bottlenecks have a number of pores ($\sim$6-7) which is higher than that of their aligned counterparts (4). This result confirms that smaller κ_{eff}, within configurations with the same porosity, can be achieved with anisotropic pore lattices, where the density of pores is higher along the Cartesian direction orthogonal to the applied temperature gradient [14, 15]. The introduction of a simple descriptor can

be used to estimate the ordering of the thermal conductivity of different samples with disordered pores [7, 13]

REPEATED-BOTTLENECK ALGORITHM

Last, we devise a method to quantify the influence of the set of pores composing the bottleneck on κ_{eff}. To this end, we use the identified bottlenecks to build a new set of configurations, closely related to the ones analyzed in the previous sections. The key idea is based on the following steps: 1) we create a random configuration as in the first section and 2) identify its bottleneck. 3) Then, we select the corresponding set of pores that created the bottleneck and repeat them along the heat flux direction while keeping the porosity fixed. We refer to this method as "repeated bottleneck". In the upper half of Fig. 5, we plot the thermal conductivity of the new configurations (κ^1_{eff}) normalized by κ^0_{eff}, i.e. the thermal conductivity of the "parent" configurations. 70% of the structures decrease in thermal transport by an average of 30 %. A further iteration of our algorithm shows that very few new bottlenecks are formed in the new structures, hence the convergence is achieved in one iteration, i.e. $\kappa^2_{eff} \approx \kappa^1_{eff}$. According to the lower part of Fig. 5, we first note that new configurations have wider distributions. In fact, the parent configurations with small d have κ_{eff} dictated by their bottleneck. Hence, their bottlenecks are reinforced in the corresponding new configurations, with consequent degradation in κ_{eff}. In the other extreme, repeating a "weak" bottleneck, i.e. with large d, introduces a significant view-factor, causing an increase in thermal transport. The size peculiarity of the square pores leads to small view factors for a wider range of d, so that the tail of the distribution for small values of κ_{eff} is higher than that for high values. For the DC case, the two tails are almost fully symmetric. As expected, for all cases, the average value of $\kappa^{(1)}_{eff}$ is lower than that of $\kappa^{(0)}_{eff}$. In fact, by definition, the value of d is generally smaller than the other pore-pore distances for a given configuration, so repeating the bottleneck leads mostly to a degradation in κ_{eff}. The repeated-bottleneck algorithm demonstrates the important role of the bottleneck pores in dictating κ_{eff} and offers a practical way of classifying strong and weak phonon bottlenecks. Further details on configurations resulting from the repeated-bottleneck algorithm are reported in the SI.

CONCLUSION

In summary, by performing high-throughput calculations of thermal transport in disordered porous materials we have quantified the effect of the randomness in pore arrangement on the thermal conductivity. Furthermore, we have devised a method to identify the set of special
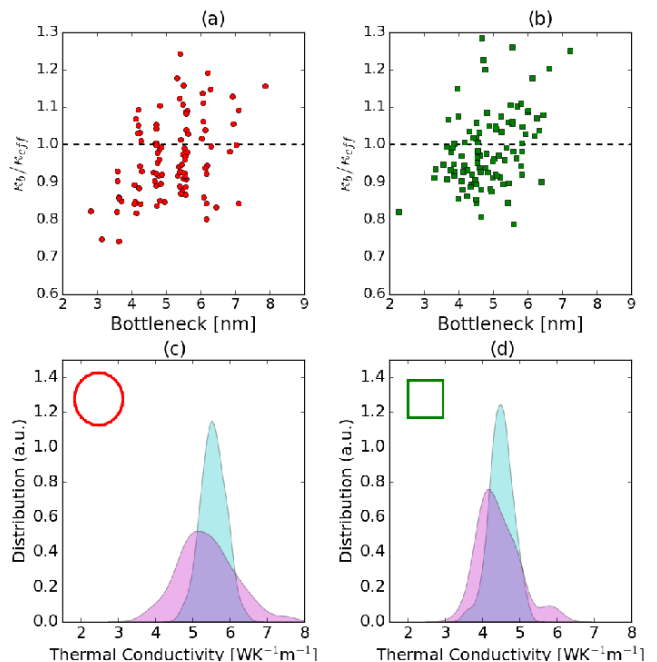

FIG. 5. The ratio between κ_{eff} of the optimized configuration and that of the original configuration for DC (a) and DS (b). On average, 70% of the values are below 1. The κ_{eff} distributions of the optimized configurations for DC and DS are shown in (c) and (d), respectively. The superposition with the distributions for the original configuration emphasizes the low-κ_{eff} configurations introduced by the repeated-bottleneck approach.

pores composing the phonon-bottleneck, potentially empowering experimentalists with a simple tools to assess thermal conductivity in realistic, disordered porous materials. Elaborating upon such a concept, we developed the repeated-bottleneck method, an approach that classifies weak and strong bottlenecks.

* romanog@mit.edu
† jcg@mit.edu

[1] D. M. Rowe, ed., *CRC Handbook of Thermoelectrics* (CRC Press, Boca Raton, FL, 1995).
[2] B. Liao, B. Qiu, J. Zhou, S. Huberman, K. Esfarjani, and G. Chen, Phys. Rev. Lett. **114**, 115901 (2015).
[3] K. Esfarjani, G. Chen, and H. T. Stokes, Phys. Rev. B **84**, 085204 (2011).
[4] P. E. Hopkins, C. M. Reinke, M. F. Su, R. H. Olsson, E. A. Shaner, Z. C. Leseman, J. R. Serrano, L. M. Phinney, and I. El-Kady, Nano Lett. **11**, 107 (2011).
[5] D. Song and G. Chen, Appl. Phys. Lett. **84**, 687 (2004).
[6] J. Lee, J. Lim, and P. Yang, Nano Lett. **15**, 3273 (2015).
[7] J. Tang, H.-T. Wang, D. H. Lee, M. Fardy, Z. Huo, T. P. Russell, and P. Yang, Nano Lett. **10**, 4279 (2010).
[8] J.-K. Yu, S. Mitrovic, D. Tham, J. Varghese, and J. R. Heath, Nat. Nanotechnol. **5**, 718 (2010).
[9] Q. Hao, G. Chen, and M.-S. Jeng, J. Appl. Phys. **106**, 114321 (2009).
[10] J.-H. Lee, G. A. Galli, and J. C. Grossman, Nano Lett. **8**, 3750 (2008).
[11] G. Romano and J. C. Grossman, J. Heat Transf. **137**, 071302 (2015).
[12] G. Romano and J. C. Grossman, Appl. Phys. Lett. **105**, 033116 (2014).
[13] B. D. Smith, J. J. Patil, N. Ferralis, and J. C. Grossman, ACS Appl. Mater. Interfaces **8**, 8043 (2016).
[14] S. Wolf, N. Neophytou, Z. Stanojevic, and H. Kosina, J. Electron. Mater. **43**, 3870 (2014).
[15] S. Wolf, N. Neophytou, and H. Kosina, J. Appl. Phys. **115**, 204306 (2014).
[16] G. Romano, K. Esfarjani, D. A. Strubbe, D. Broido, and A. M. Kolpak, Phys. Rev. B **93**, 035408 (2016).
[17] D. Broido, M. Malorny, G. Birner, N. Mingo, and D. Stewart, Appl. Phys. Lett. **91**, 231922 (2007).
[18] C. Geuzaine and J.-F. Remacle, Int. J. Numer. Meth. Eng. **79**, 1309 (2009).
[19] T. Abe, J. Comput. Phys. **131**, 241 (1997).
[20] G. Romano and A. Di Carlo, IEEE Trans. Nanotechnol. **10**, 1285 (2011).
[21] W. Li, J. Carrete, N. A. Katcho, and N. Mingo, Comput. Phys. Commun. **185**, 1747 (2014).
[22] J. Ziman, *Electrons and Phonons* (Oxford University Press (OUP), 2001).
[23] J. R. Howell, M. P. Menguc, and R. Siegel, *Thermal radiation heat transfer* (2010).
[24] PyClipper 1.0.2. https://pypi.python.org/pypi/pyclipper .
[25] D. B. Johnson, SIAM J. Comput. **4**, 77 (1975).
[26] NetworkX. https://networkx.github.io/index.htm .
[27] J. Carrete, W. Li, N. Mingo, S. Wang, and S. Curtarolo, Phys. Rev. X **4**, 011019 (2014).